

THE AGES OF HIGH MASS X-RAY BINARIES IN NGC 2403 AND NGC 300

BENJAMIN F. WILLIAMS¹, BREANNA A. BINDER¹, JULIANNE J. DALCANTON¹, MICHAEL ERACLEOUS², ANDREW DOLPHIN³

Draft version April 25, 2021

ABSTRACT

We have examined resolved stellar photometry from *HST* imaging surrounding 18 high-mass X-ray binary (HMXB) candidates in NGC 300 and NGC 2403 as determined from combined *Chandra*/*HST* analysis. We have fit the color-magnitude distribution of the surrounding stars with stellar evolution models. All but one region in NGC 300 and two in NGC 2403 contain a population with an age between 20 and 70 Myr. One of the candidates is the ultraluminous X-ray source (ULX) in NGC 2403, which we associate with a 60 ± 5 Myr old population. These age distributions provide additional evidence that 16 of these 18 candidates are HMXBs. Furthermore, our results suggest that the most common HMXB age in these galaxies is 40–55 Myr. This preferred age is similar to observations of HMXBs in the Small Magellanic Cloud, providing new evidence of this formation timescale, but in higher metallicity populations. We suggest that this preferred HMXB age is the result of the fortuitous combination of two physical effects. First, this is the age of a population when the greatest rate of core-collapse events should be occurring, maximizing neutron star production. Second, this is the age when B stars are most likely to be actively losing mass. We also discuss our results in the context of HMXB feedback in galaxies, confirming HMXBs as a potentially important source of energy for the interstellar medium in low-mass galaxies.

Subject headings: pulsars: general — stars: early-type — X-rays: binaries — galaxies: individual (NGC-300, NGC-2403)

1. INTRODUCTION

High mass X-ray binaries (HMXBs) provide one of the best probes of the endpoint of massive stars' evolution. These binaries consist of a compact object accreting material from a massive companion, allowing stringent lower limits to be placed on the mass of the compact object progenitor. Furthermore, the high luminosity of the companion allows the potential for radial velocity measurements to determine the binary mass ratio. In cases where the HMXB is X-ray bright, the X-ray variability and spectral properties yield information about the nature of the accretion flow onto the compact object.

Because HMXBs are such powerful laboratories for understanding both high-mass and binary stellar evolution, the known X-ray bright systems in the Galaxy have been studied in great detail (e.g. Tanaka & Shibazaki 1996; Lewin & van der Klis 2006; Remillard & McClintock 2006, and references therein). The Small Magellanic Cloud's (SMC's) rich HMXB population (Yokogawa et al. 2003) has also been well-studied, providing a probe of HMXBs at low metallicity (Antoniou et al. 2009a,b, 2010).

Measurements of formation timescales of HMXBs provide key constraints for binary evolution models. Determining the ages of HMXB systems in the Milky Way is difficult due to distance uncertainties and high extinction, as most HMXBs are in the Galactic plane. The most fruitful studies to date have focused the SMC, which find a typical formation timescale of 25–60 Myr (Antoniou et al. 2010). This timescale would

explain the SMC's richness in HMXB, since it experienced a strong episode of star formation ~ 50 Myr ago (Shtykovskiy & Gilfanov 2007; Antoniou et al. 2010).

It is difficult to determine conclusively why HMXBs would preferably form on a ~ 50 Myr timescale. One possible explanation is that this is the time when B stars – the most common type of secondary in HMXBs – shed mass at the highest rate. In the Galaxy, B star activity reaches a maximum between 25 and 80 Myr (McSwain & Gies 2005), in broad agreement with the HMXB age distribution in the SMC.

Herein, we turn our attention to two new galaxies, NGC 300 and NGC 2403, where we may learn about the timescales of HMXB formation at a metallicity that is higher than the SMC and more characteristic of the older stars in galactic disks ($-0.7 \lesssim [\text{Fe}/\text{H}] \lesssim -0.3$, Bresolin et al. 2009; Gogarten et al. 2010; Garnett et al. 1997; Barker et al. 2012; Williams et al. 2013), which may play a role in early HMXB feedback (Justham & Schawinski 2012). NGC 300 is a SA(s)d type, at a distance of 2.0 Mpc (Dalcanton et al. 2009). It is nearly face-on (42° Carignan 1985), and of intermediate metallicity. Thus the complications of dust extinction are minimized, and it probes an interesting mass-metallicity regime between the SMC and the Galaxy. NGC 2403 is a similar type galaxy with a somewhat larger mass, distance (3.3 Mpc Dalcanton et al. 2009), with similar metallicity, and dust content (Williams et al. 2013).

Recently, deep *Chandra* observations of NGC 300 and NGC 2403 were analyzed as part of the Chandra Local Volume (CLV) survey (Binder et al. 2012, B. Binder et al., in preparation). This study included a new method for identifying strong HMXB candidates using a combination of the *Chandra* data and overlapping *HST* imaging

¹Department of Astronomy, Box 351580, University of Washington, Seattle, WA 98195; ben@astro.washington.edu; bbinder@astro.washington.edu; jd@astro.washington.edu

²Pennsylvania State University; mce@astro.psu.edu

³Raytheon; adolphin@raytheon.com

available from the ACS Nearby Galaxy Treasury project (ANGST Dalcanton et al. 2009). In total, 18 HMXB candidates were found within the boundaries of deep *HST* images of NGC 300 and NGC 2403. These X-ray sources all have a blue ($V-I < 0$ equivalent) optical counterpart candidates that fall within the *Chandra* error circle. The brightest of these candidates were taken to produce the histogram of optical magnitudes in Figure 1. The *HST* data provide deep resolved stellar photometry near the HMXB positions, which we fit with stellar evolution models to search for young coeval populations to constrain the HMXBs’ ages.

The paper is organized into 4 sections. Section 2 discusses the data and analysis techniques used to make our age distribution measurements. Section 3 discusses the results of the measurements, including implications concerning the formation of HMXBs. Finally, Section 4 provides a brief summary of our conclusions. We assume distances of 2.0 Mpc and 3.2 Mpc to NGC 300 and NGC 2403 respectively throughout the paper, and all X-ray luminosities are quoted for the 0.35–8.0 keV energy range.

2. DATA REDUCTION AND ANALYSIS

There were 4 relevant archival *HST* fields in NGC 300 and 2 in NGC 2403. Two of these fields were part of the ANGST project (GO-10915; NGC0300-WIDE1, NGC0300-WIDE2 Dalcanton et al. 2009), the other four were taken from the *HST* archive (GO-9492 – NGC300-1, NGC300-6; GO-10579 – NGC2403-X1; GO-10182 – SN-NGC2403-PR). The footprints of these fields are shown on Digitized Sky Survey images of NGC 300 and NGC 2403 in Figure 1. The details of the filters, exposure times, and depths are given in Table 1.

Through cross-correlation of *Chandra* and *HST* catalogs Binder et al. (2012) found 5 HMXB candidates in NGC 300 and 13 HMXB candidates in NGC 2403 that fell within *HST/ACS* imaging fields. The distributions of optical magnitudes and X-ray luminosities of these candidates are shown in Figure 1. The vast majority of the optical counterpart candidates have optical magnitudes that are typical of B-type stars, and the X-ray luminosities are typical of HMXBs in outburst. The *Chandra* data are not sensitive enough to reach quiescent HMXBs at the distance of NGC 300. One source is clearly ultraluminous. This is the NGC 2403 ULX, which has an optical counterpart candidate with $M_{F555W} = -2.6$.

2.1. Photometry

All photometry and artificial star tests were measured and performed as described by the ANGST project paper (Dalcanton et al. 2009). Briefly, all photometry was performed using DOLPHOT, an updated version of HST-phot optimized for ACS photometry. Photometry was culled based on signal-to-noise ratio and the quality parameters of sharpness and crowding, as described in Dalcanton et al. (2009). We selected only the photometry from a circular region with a radius of 50 pc around the positions of the HMXBs (5.1'' and 3.2'' in NGC 300 and NGC 2403, respectively). The CMDs of these regions are shown in Figures 2 and 3. Fake star tests were taken from larger regions (25'' and 15'') in order to gain a large number of tests to improve statistics of the photometric uncertainties and completeness as a function of

color and brightness. The *HST* images of one source in each galaxy are given in Figure 1, showing that the stellar density and extinction does not vary strongly within these relatively small spatial scales.

2.2. Color-Magnitude Diagram Fitting

We fit the color-magnitude diagrams for each of the fields in our study using the software package MATCH (Dolphin 2002). The overall technique for our fitting, as it has been applied for all ANGST papers, is described in detail in Williams et al. (2009); however, there have been some changes in the method for uncertainty estimation. Output star formation rates are renormalized to a Kroupa (2001) initial mass function. Furthermore, we find the best-fitting mean extinction to each location with the distance fixed to 2.0 Mpc and 3.2 Mpc for NGC 300 and NGC 2403, respectively (Dalcanton et al. 2009). We found the best fitting extinction to be consistent with the foreground value from Schlegel et al. (1998). In addition, we attempted to improve the model fits by including differential reddening in the model Hess diagrams by spreading the model photometry along the reddening line using the MATCH `dAv` flag; however, we found no improvement and therefore no evidence for significant differential reddening in these locations, suggesting these are not extremely young active regions associated with O-type stars. With these distance and extinction values applied, we then run a series of 100 Monte Carlo (MC) tests.

To assess the full combination of systematic errors due to model deficiencies as well as random errors due to the depth and size of the sample, realizations of the best-fitting model solution are fitted with the models shifted in bolometric magnitude and effective temperature (Dolphin 2012). These shifts account for the uncertainties due to any potential systematic offsets between the data and models. This total uncertainty was measured for one location to assess the total uncertainties in the rest of outer portions of the galaxy.

When searching for differences between different locations in the same galaxy, systematic uncertainties due to offsets between the models and the data are not of concern, since these systematics will affect all fields. To estimate the *relative* uncertainty for differences between two location analyzed using the same models, we need only to assess the random errors due to the depth and size of the sample. Therefore, for the other locations, our MC error analysis did not include shifts between the models and data.

3. RESULTS AND DISCUSSION

3.1. Source 42: The ULX

One interesting test case is NGC 2403 source 42, which is a well-studied ULX that is thought to have a black hole primary (Fabbiano & Trinchieri 1987; Swartz et al. 2004; Feng & Kaaret 2005; Isobe et al. 2009). The black hole mass is estimated from *Suzaku* X-ray spectra to be 10–15 M_{\odot} , assuming radiation near the Eddington limit (Isobe et al. 2009). There is no confirmed optical counterpart. Our analysis suggests that it resides in a region with no stars younger than 50 Myr, but with a significant population of stars with ages 60 ± 5 Myr. Since the progenitor of the black hole likely had a main sequence lifetime of $\lesssim 10$ Myr, our result suggests that

this ULX either has had a very long X-ray lifetime compared to the lifetime of the primary, or the ULX is so bright now because it has a secondary that is in a state of rapid mass-loss, as in the model of King et al. (2001). *Spitzer* imaging from the SINGS (Kennicutt et al. 2003) program shows no obvious counterpart in the near or mid infrared, so it does not appear to be an IR-bright asymptotic giant branch star, shedding its envelope. In any case, if the ULX is associated with this 60 Myr population, then the secondary likely has a zero-age main-sequence mass of $\lesssim 7 M_{\odot}$.

3.2. A Peak in the HMXB Age Distribution

Turning now to the broader sample, in Figures 4 and 5, we show the recent star formation histories (SFHs) for the regions surrounding all 18 HMXB candidates. For reference, we highlight the age range between 30 and 60 Myr. All but 3 (N300-95, N2403-39, and N2403-85) show a significant peak in between 20 and 70 Myr. One of these (NGC2403-85) shows a population of 10–20 Myr, and therefore is still a potential HMXB. HMXBs are expected to appear in populations even younger than 10–20 Myr. The population synthesis models of Van Bever & Vanbeveren (2000) show that substantial numbers of HMXBs appear 4-5 Myr after the beginning of star formation. A possible evolutionary scenario for the formation of such an HMXB on a time scale of 5-6 Myr is described in Belczynski & Taam (2008, assuming that the binary survives the first supernova). Observationally, a case in point is provided by the Galactic cluster Westerlund 1, which has an age of ~ 4 Myr. This cluster has several Wolf-Rayet binaries (potential progenitors of HMXBs), one candidate HMXB, and a magnetar, indicating that a number of compact objects have already formed from supernovae (see Muno et al. 2006; Clark et al. 2008).

N300-95 has a 100 Myr population, pushing the old-age limits for an HMXB, and N2403-39, while showing no significant population younger than 100 Myr, has upper limits that allow the possibility of some young stars in the region. The X-ray sources in regions with very little recent star formation could also be LMXBs, since all of these regions also contain significant old populations. However, if for example, N2403-39 is an LMXB, then the counterpart is not the blue star that falls in the Chandra error circle.

When we combine the results from all of the candidates in our sample, as shown in Figure 6, we find a prominent enhancement in the age distribution at 40–55 Myr. This result provides more evidence that 40–55 Myr is a common age for HMXB systems, and therefore may represent the post star-formation epoch with the largest number of HMXBs per unit stellar mass formed. Furthermore, this epoch would presumably also be the interval of maximum feedback from HMXB jets, outflows, and high-energy radiation.

To quantify the likelihood of such a peak in a summed age distribution appearing by chance, we fit photometry from a control sample. This control sample consisted of photometry drawn from 18 regions within $0.5''$ of randomly drawn bright blue stars in the *HST* fields. We required the same number of regions per field as the HMXB sample. We ran these random locations through our fitting technique and summed the results, finding no clear

peak in the age distribution (Figure 6). We then ran this test 1000 times to see if we ever randomly recovered a peak similar to that seen in the age distribution of the HMXB sample. We found that 1.5% of our trials resulted in a peak of at least a factor of 2.35 in 2 adjacent bins between the ages of 20 and 140 Myr (as seen in the HMXB sample). A smaller number (0.4%) of our trials had such peaks as old as the 40–55 Myr peak seen in the HMXB distribution. Thus, a peak like that seen in the HMXB sample is a 3σ outlier in our trials, roughly consistent with the uncertainty estimates shown in Figure 6.

3.3. Implications for Binary Evolution Theory

The standard model of massive binary evolution suggests that in a massive binary (e.g. B and O stars or A and O stars), the more massive star evolves first and transfers mass to the less massive companion when it overflows its Roche lobe. The core of the massive star subsequently collapses, forming a neutron star or black hole. If the binary remains bound after the core-collapse supernova, it may become an HMXB (e.g. van den Heuvel & De Loore 1973; van den Heuvel 1976).

After mass accretion, the less massive star is spun up due to the addition of high angular momentum material (Pols et al. 1991; van Bever & Vanbeveren 1997), and subsequent evolution occurs at higher temperatures (e.g., van Bever & Vanbeveren 1998). The rapid rotation pushes the wind of this hot star into the equatorial plane and leads to the formation of an equatorial outflow disk (Bjorkman & Cassinelli 1993), which makes this an active B-star (Be star). As this mass is transferred back to, and accreted by, the compact object, X-ray emission is produced and the binary becomes a Be-HMXB (Van Bever & Vanbeveren 2000).

Because the B-star is rapidly rotating, the mass outflow is localized in the equatorial plane. This “outflow disk” increases the mass transfer efficiency. The resulting X-ray luminosity is low a large fraction of the time ($< 10^{35}$ erg s^{-1}). However, these systems can sometimes reach luminosities of 10^{37} erg s^{-1} because the outflow disk is unstable and can have episodes of enhanced outflow (e.g., Reig et al. 2007), which lead to an increase in the accretion rate (and X-ray luminosity) of the compact object.

Given this model of HMXB formation, one might expect a correspondence between HMXB ages and B-star evolution. Observations suggest that the fraction of active B stars (Be stars) peaks at 25–80 Myr (McSwain & Gies 2005). Our measurements suggest that the fraction of HMXBs appears to peak at 40–55 Myr, in good agreement. Thus, the activity cycle of B-stars appears to be involved in the observed peak in the age distribution.

The 40–55 Myr timescale is also associated with a possible peak in the neutron star production rate. Current theory and observations suggest that stars with zero age main-sequence masses of $7-8 M_{\odot}$ are the lowest mass stars to undergo core-collapse to form neutron stars (e.g., Jennings et al. 2012). According to the initial mass function (Kroupa 2001), for a given star forming episode, there are always more lower mass stars than higher mass ones. Therefore the highest rate of core-collapse likely occurs when the lifetime of $7-8 M_{\odot}$ stars has been reached.

This lifetime is 40–55 Myr according to, for example, the Padova stellar evolution models (Marigo et al. 2008). Therefore, the production rate of neutron stars is likely involved in the observed peak in the age distribution as well. Thus, both the mass-loss by B stars and the number of potential HMXB systems are at a maximum at ~ 50 Myr after star formation, conspiring to form the peak that we see in the HMXB age distribution.

3.4. Implications for HMXB feedback

Recent attempts to include baryonic physics in galaxy formation models and simulations have found that the treatment of feedback, energy injection into the interstellar gas, plays an important role in shaping not only the mass function (e.g., Benson et al. 2003) and star formation histories of galaxies (e.g., Stinson et al. 2007; Quillen & Bland-Hawthorn 2008), but also their dark matter halo density profiles (Governato et al. 2010). The necessary timescale and energetics of the feedback required to reproduce observed galaxy properties are complex, and as a result, the origin of the feedback remains controversial. At least part of the necessary feedback appears to be related to star formation, especially in low mass galaxies where no active nucleus is present.

We note that the peak we observe in HMXB activity ~ 50 Myr after star formation is generally consistent with HMXBs contributing significantly to the feedback resulting from star formation. For example, Justham & Schawinski (2012) suggest that the cumulative energy input from HMXBs can be similar to that from SNe, and they point out that HMXB feedback may have the appropriate delay time required to produce episodic star formation histories of low mass galaxies. Our results suggest that feedback from HMXBs is maximized ~ 50 Myr after star formation, roughly consistent with the delay time required by some models (e.g., Quillen & Bland-Hawthorn 2008). However, the delay between star formation and the transfer of SNe energy into the ISM is a similar length at low SN-rates (Dib et al. 2006), therefore both processes should be considered potentially important to the feedback budget.

Furthermore, Stilp et al. (2013) recently discovered a correlation between the energetics of the neutral interstellar medium (ISM) and the star formation rate 30–40 Myr earlier. This result suggests that the energy associated with star formation is transferred to the neutral ISM with roughly this delay time. The consistency of this timescale with the delay time of HMXB feedback provides further evidence that feedback from both HMXBs and SNe are potentially important for regulating star formation in low-mass galaxies.

While the observed delay time between star formation and HMXB activity makes HMXB feedback potentially important in low-mass galaxies, the relatively low energies associated with HMXBs, makes them only minor contributors to feedback in more massive systems. Massive galaxies contain supermassive black holes. Central black holes have masses of $M_{BH} \sim 1.4 \times 10^{-3} M_{gal}$ (Fabian 2012). Assuming the energy released in producing the central black hole is $E_{BH} = 0.1 M_{BH} c^2$, putting E_{BH} in units of ergs and M_{BH} in units of so-

lar masses yields $E_{BH} = 2.5 \times 10^{50} M_{gal} / M_{\odot}$. We can also determine E_{HMXB} as a function of M_{gal} by assuming that E_{HMXB}/t , where t has units of seconds, is equivalent to the X-ray luminosity (L_X), and setting $SFR_s \times t < M_{gal}$, where SFR_s is the star formation rate in units of $M_{\odot} s^{-1}$. We can now apply the relation between L_X and SFR from Grimm et al. (2003), which is $L_X = 6.7 \times 10^{39} SFR$, where L_X is in units of erg s^{-1} and SFR is in units of $M_{\odot} \text{ yr}^{-1}$. Substituting SFR_s for SFR yields $L_X = 2.1 \times 10^{47} SFR_s$; then applying $M_{gal}/t > SFR_s$ and $E_{HMXB}/t = L_X$ gives $E_{HMXB} < 2.1 \times 10^{47} M_{gal} / M_{\odot}$. Thus, $E_{BH} / E_{HMXB} \gtrsim 10^3$, making E_{HMXB} a very minor contributor to the global evolution of massive galaxies.

4. CONCLUSIONS

We have performed model fits to the color-magnitude distribution of the stars within 50 pc of HMXB candidates in NGC 300 and NGC 2403 that have adequate *HST* archival data. The ULX in NGC 2403 is one of these sources, and it appears to be associated with a population of 60 ± 5 Myr in age. The total of the resulting recent star formation histories show a significant peak between 40 and 55 Myr. This peak is coincident with the timescale for HMXB formation as seen in the SMC. Using these results, we can infer that N300-5, N300-13, N300-22, N2403-22, N2403-42, N2403-44, N2403-55, N2403-57, N2403-63, N2403-69, N2403-70, and N2403-84 are the strongest HMXB candidates, and that the timescale for maximum HMXB activity is similar to that seen in the SMC.

The formation of an HMXB requires the production of a neutron star or black hole through a core-collapse supernova of the primary and mass-loss by the secondary to fuel the accretion process. Due to a fortuitous coincidence, both the age of a population when B-star mass loss is at a maximum (e.g., McSwain & Gies 2005) and the age when neutron star production is a maximum (e.g., Jennings et al. 2012) are ~ 50 Myr. Thus, the peak we observe in the HMXB age distribution strengthens recent observations and theory of the evolution of massive stars in binary systems.

Finally, this timescale for the peak of HMXB activity after the onset of star formation may help to address some open questions in the interplay between star formation and galaxy evolution. First, it is consistent with the delay between star formation and feedback processes required by some models to reproduce episodic star formation in low-mass galaxies. Second, it is consistent with the delay time between star formation and delivery of energy to the ISM observed in nearby low-mass galaxies.

Support for this work was provided through Chandra Award Number AR2-13005X issued by the Chandra X-Ray Observatory Center, which is operated by the Smithsonian Astrophysical Observatory for and on behalf of the National Aeronautics Space Administration under contract NAS8-03060. Additional funding was provided by grants GO-10915 and GO-11986 from the Space Telescope Science Institute, which is operated by the Association of Universities for Research in Astronomy, Incorporated, under NASA contract NAS5-26555.

REFERENCES

- Antoniou, V., Hatzidimitriou, D., Zezas, A., & Reig, P. 2009a, *ApJ*, 707, 1080
- Antoniou, V., Zezas, A., Hatzidimitriou, D., & Kalogera, V. 2010, *ApJ*, 716, L140

- Antoniou, V., Zezas, A., Hatzidimitriou, D., & McDowell, J. C. 2009b, *ApJ*, 697, 1695
- Barker, M. K., Ferguson, A. M. N., Irwin, M. J., Arimoto, N., & Jablonka, P. 2012, *MNRAS*, 419, 1489
- Belczynski, K., & Taam, R. E. 2008, *ApJ*, 685, 400
- Benson, A. J., Bower, R. G., Frenk, C. S., Lacey, C. G., Baugh, C. M., & Cole, S. 2003, *ApJ*, 599, 38
- Binder, B., et al. 2012, *ApJ*, 758, 15
- Bjorkman, J. E., & Cassinelli, J. P. 1993, *ApJ*, 409, 429
- Bresolin, F., Gieren, W., Kudritzki, R.-P., Pietrzyński, G., Urbaneja, M. A., & Carraro, G. 2009, *ApJ*, 700, 309
- Carignan, C. 1985, *ApJS*, 58, 107
- Clark, J. S., Muno, M. P., Negueruela, I., Dougherty, S. M., Crowther, P. A., Goodwin, S. P., & de Grijs, R. 2008, *A&A*, 477, 147
- Dalcanton, J. J., et al. 2009, *ApJS*, 183, 67
- Dib, S., Bell, E., & Burkert, A. 2006, *ApJ*, 638, 797
- Dolphin, A. E. 2002, *MNRAS*, 332, 91
- Dolphin, A. E. 2012, *ApJ*, 751, 60
- Fabbiano, G., & Trinchieri, G. 1987, *ApJ*, 315, 46
- Fabian, A. C. 2012, *ARA&A*, 50, 455
- Feng, H., & Kaaret, P. 2005, *ApJ*, 633, 1052
- Garnett, D. R., Shields, G. A., Skillman, E. D., Sagan, S. P., & Dufour, R. J. 1997, *ApJ*, 489, 63
- Gogarten, S. M., et al. 2010, *ApJ*, 712, 858
- Governato, F., et al. 2010, *Nature*, 463, 203
- Grimm, H.-J., Gilfanov, M., & Sunyaev, R. 2003, *MNRAS*, 339, 793
- Isobe, N., et al. 2009, *PASJ*, 61, 279
- Jennings, Z. G., Williams, B. F., Murphy, J. W., Dalcanton, J. J., Gilbert, K. M., Dolphin, A. E., Fouesneau, M., & Weisz, D. R. 2012, *ApJ*, 761, 26
- Justham, S., & Schawinski, K. 2012, *MNRAS*, 423, 1641
- Kennicutt, R. C., Jr., et al. 2003, *PASP*, 115, 928
- King, A. R., Davies, M. B., Ward, M. J., Fabbiano, G., & Elvis, M. 2001, *ApJ*, 552, L109
- Kroupa, P. 2001, *MNRAS*, 322, 231
- Lewin, W. H. G., & van der Klis, M. 2006, *Compact Stellar X-ray Sources*
- Marigo, P., Girardi, L., Bressan, A., Groenewegen, M. A. T., Silva, L., & Granato, G. L. 2008, *A&A*, 482, 883
- McSwain, M. V., & Gies, D. R. 2005, *ApJS*, 161, 118
- Muno, M. P., et al. 2006, *ApJ*, 636, L41
- Pols, O. R., Cote, J., Waters, L. B. F. M., & Heise, J. 1991, *A&A*, 241, 419
- Quillen, A. C., & Bland-Hawthorn, J. 2008, *MNRAS*, 386, 2227
- Reig, P., Larionov, V., Negueruela, I., Arkharov, A. A., & Kudryavtseva, N. A. 2007, *A&A*, 462, 1081
- Remillard, R. A., & McClintock, J. E. 2006, *ARA&A*, 44, 49
- Schlegel, D. J., Finkbeiner, D. P., & Davis, M. 1998, *ApJ*, 500, 525
- Shtykovskiy, P. E., & Gilfanov, M. R. 2007, *Astronomy Letters*, 33, 437
- Stilp, A. M., Dalcanton, J. J., Warren, S. R., Weisz, D., Skillman, E., Ott, J., Williams, B., & Dolphin, A. 2013, *ApJ*, submitted
- Stinson, G. S., Dalcanton, J. J., Quinn, T., Kaufmann, T., & Wadsley, J. 2007, *ApJ*, 667, 170
- Swartz, D. A., Ghosh, K. K., Tennant, A. F., & Wu, K. 2004, *ApJS*, 154, 519
- Tanaka, Y., & Shibazaki, N. 1996, *ARA&A*, 34, 607
- van Bever, J., & Vanbeveren, D. 1997, *A&A*, 322, 116
- van Bever, J., & Vanbeveren, D. 1998, *A&A*, 334, 21
- Van Bever, J., & Vanbeveren, D. 2000, *A&A*, 358, 462
- van den Heuvel, E. P. J. 1976, in *IAU Symposium*, Vol. 73, *Structure and Evolution of Close Binary Systems*, ed. P. Eggleton, S. Mitton, & J. Whelan, 35
- van den Heuvel, E. P. J., & De Loore, C. 1973, *A&A*, 25, 387
- Williams, B. F., et al. 2009, *AJ*, 137, 419
- Williams, B. F., Dalcanton, J. J., Stilp, A., Dolphin, A., Skillman, E. D., & Radburn-Smith, D. 2013, *ApJ*, 765, 120
- Yokogawa, J., Imanishi, K., Tsujimoto, M., Koyama, K., & Nishiuchi, M. 2003, *PASJ*, 55, 161

TABLE 1
SUMMARY OF DATA AND PHOTOMETRY MEASUREMENTS

Proposal	Target	Camera	Filter	Exposure (s)	Stars	$m_{50\%}$
9492	NGC300-1	ACS	F435W	1080	94793	27.51
9492	NGC300-1	ACS	F555W	1080	126857	27.45
9492	NGC300-1	ACS	F814W	1440	126857	27.10
9492	NGC300-6	ACS	F435W	1080	72509	27.46
9492	NGC300-6	ACS	F555W	1080	111850	27.38
9492	NGC300-6	ACS	F814W	1440	111850	27.07
10915	NGC0300-WIDE1	ACS	F475W	1488	201775	27.84
10915	NGC0300-WIDE1	ACS	F606W	1515	224152	27.84
10915	NGC0300-WIDE1	ACS	F814W	1542	224152	27.04
10915	NGC0300-WIDE2	ACS	F475W	1488	314579	27.29
10915	NGC0300-WIDE2	ACS	F606W	1515	363837	27.04
10915	NGC0300-WIDE2	ACS	F814W	1542	363837	26.53
10182	SN-NGC2403-PR	ACS	F475W	1200	316973	26.41
10182	SN-NGC2403-PR	ACS	F814W	700	316973	25.47
10579	NGC2403-X1	ACS	F435W	1248	154848	26.84
10579	NGC2403-X1	ACS	F606W	1248	154848	26.32

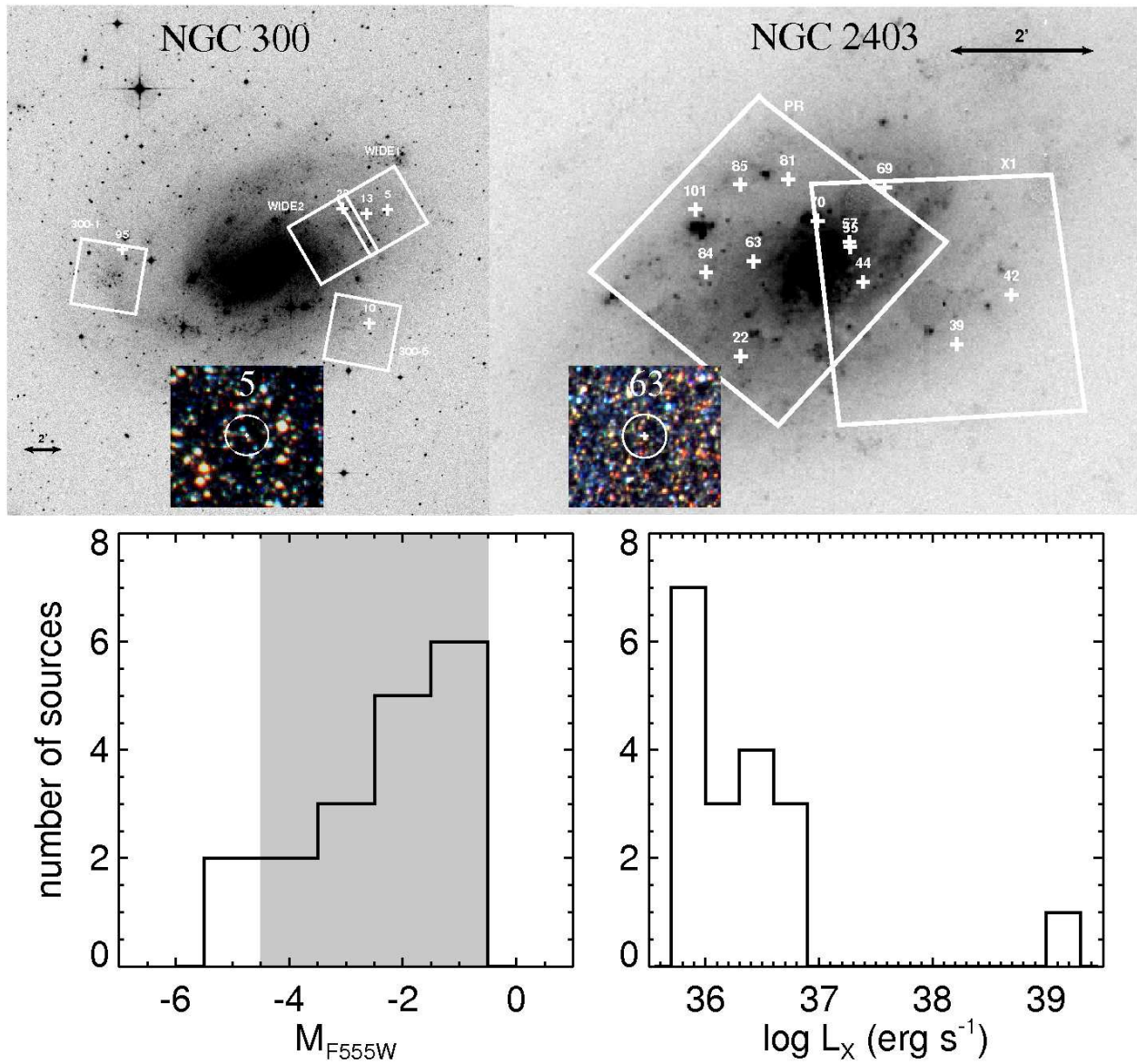


FIG. 1.— *Top*: Footprints of our sample *HST* fields shown on Digitized Sky Survey images of NGC 300 (left) and NGC 2403 (right). North is up and East is left. Fields are labeled with shortened versions of their names given in Table 1. Crosses mark the relevant HMXB candidate locations. Inset are $5''$ sections of the *HST* images around one HMXB candidate from each galaxy, to show the uniformity of the stellar density on these spatial scales. *Bottom Left*: Histogram of the absolute F555W magnitudes of the brightest optical sources coincident with the HMXB candidates in our sample. The shaded region shows the typical luminosities of B-type stars. *Bottom Right*: Histogram of the observed 0.35–8 keV X-ray luminosities of our sample. All but the ULX are in the luminosity range typical of HMXBs in outburst.

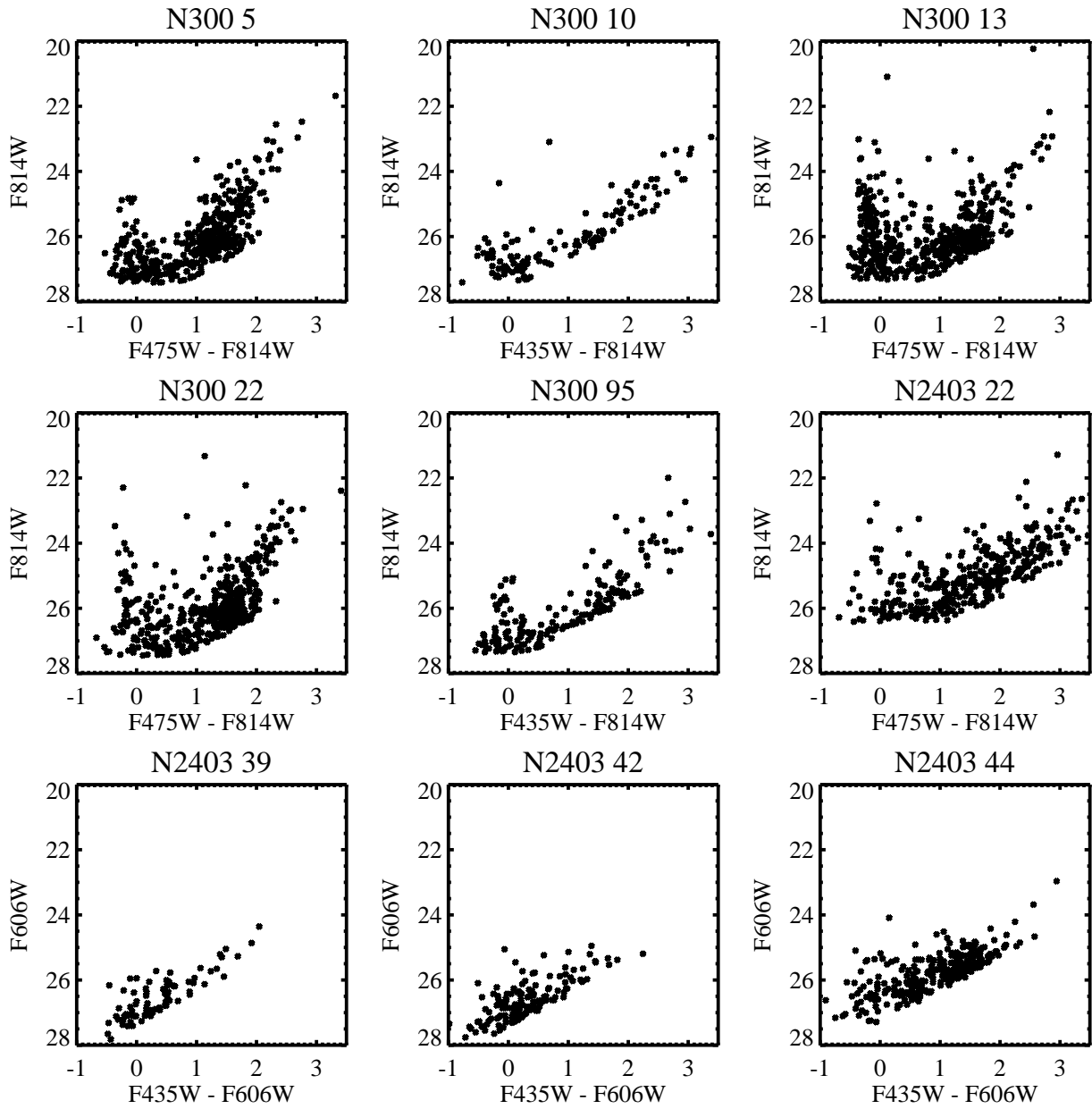


FIG. 2.— Color-Magnitude diagrams for 9 of the regions in our study. These represent all of the measured stars within 50 pc of the locations of 9 of the HMXB candidates marked with crosses in Figure 1. The diagrams extend fainter than the 50% completeness limit of the data, as stars are still measured at those magnitudes at low levels of completeness, making them unusable for our model fitting.

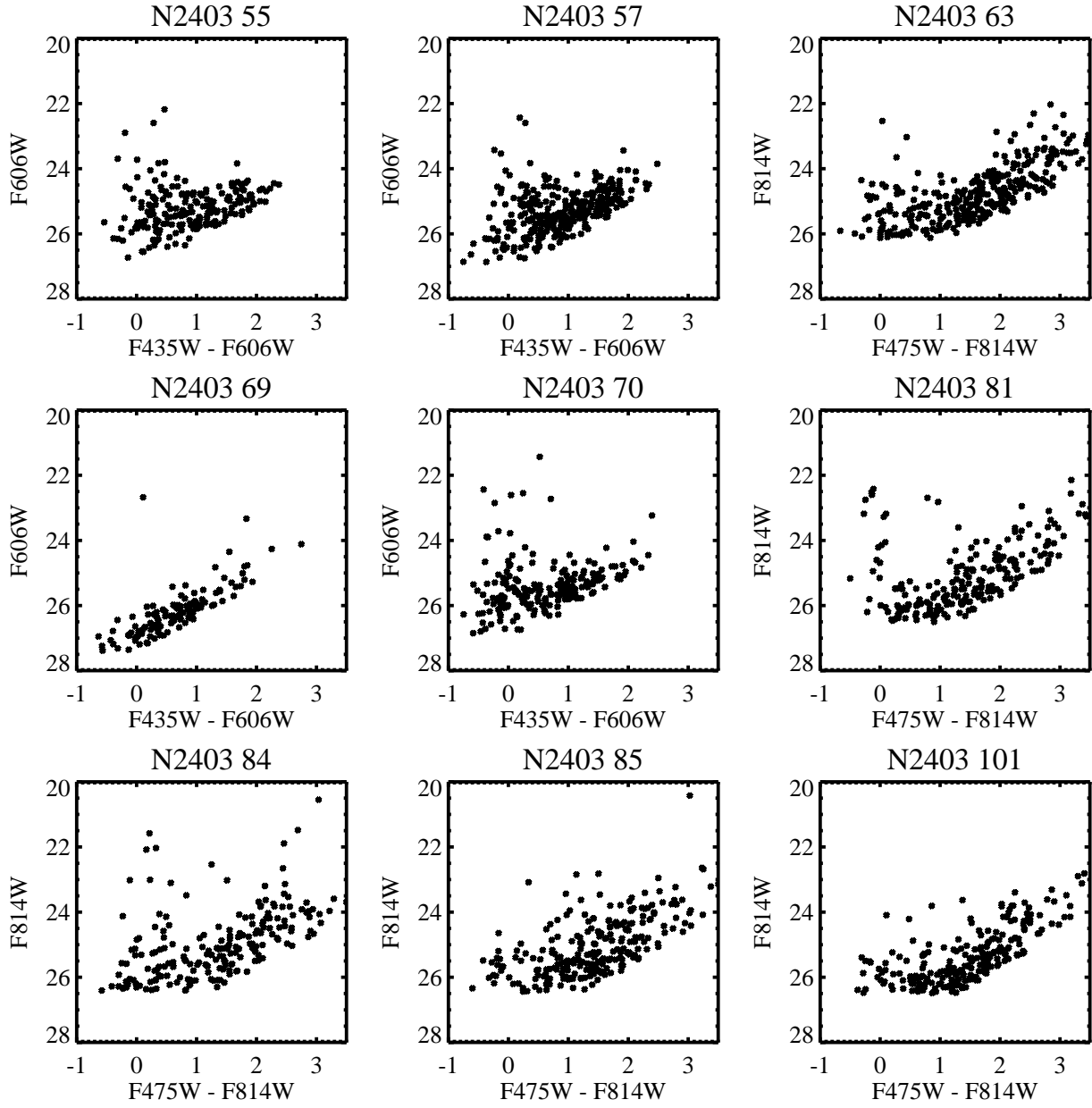


FIG. 3.— Same as Figure 2, but for the remaining 9 of the regions in our study.

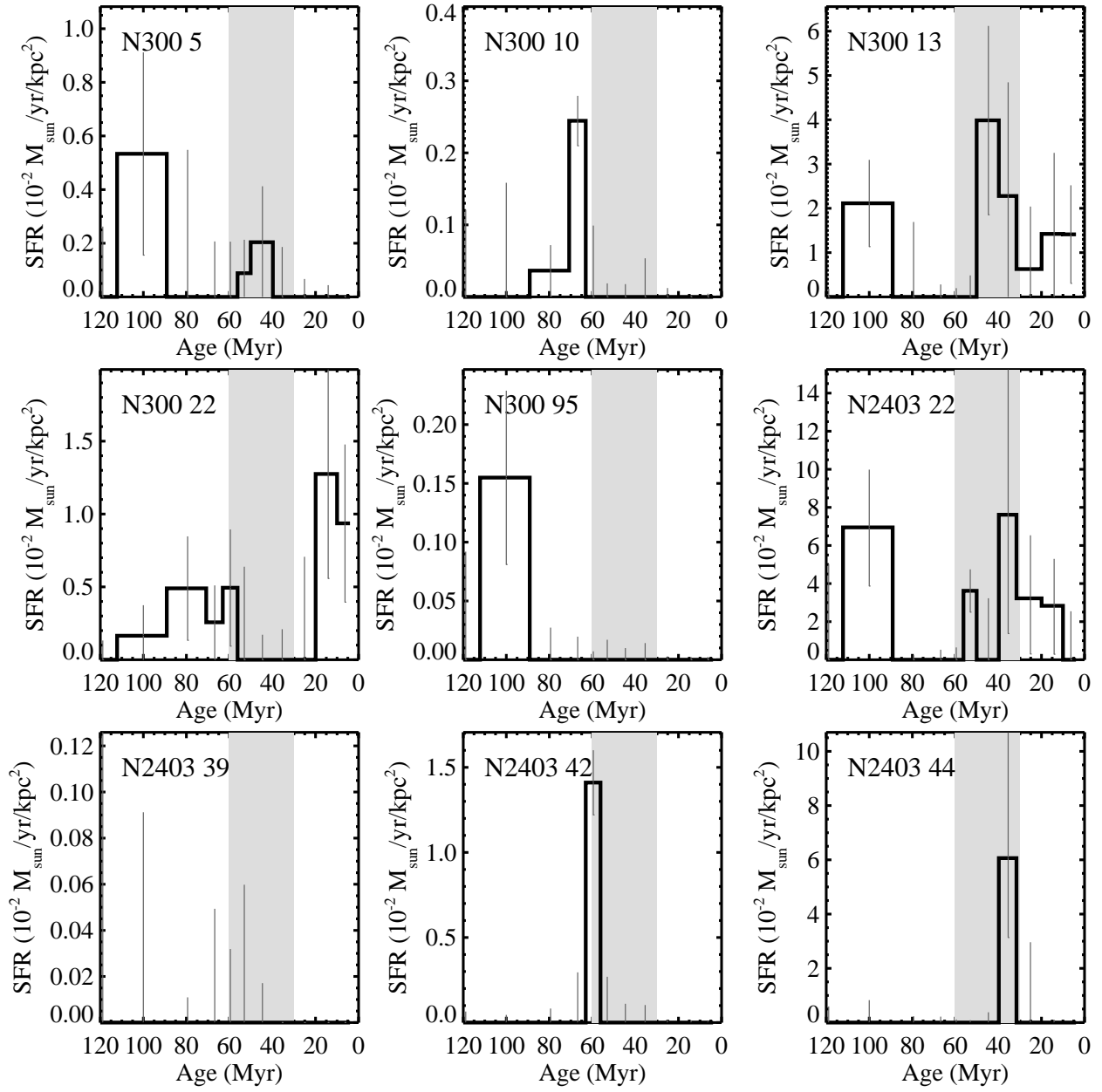


FIG. 4.— Recent SFHs resulting from model fits to the CMDs shown in Figure 2.

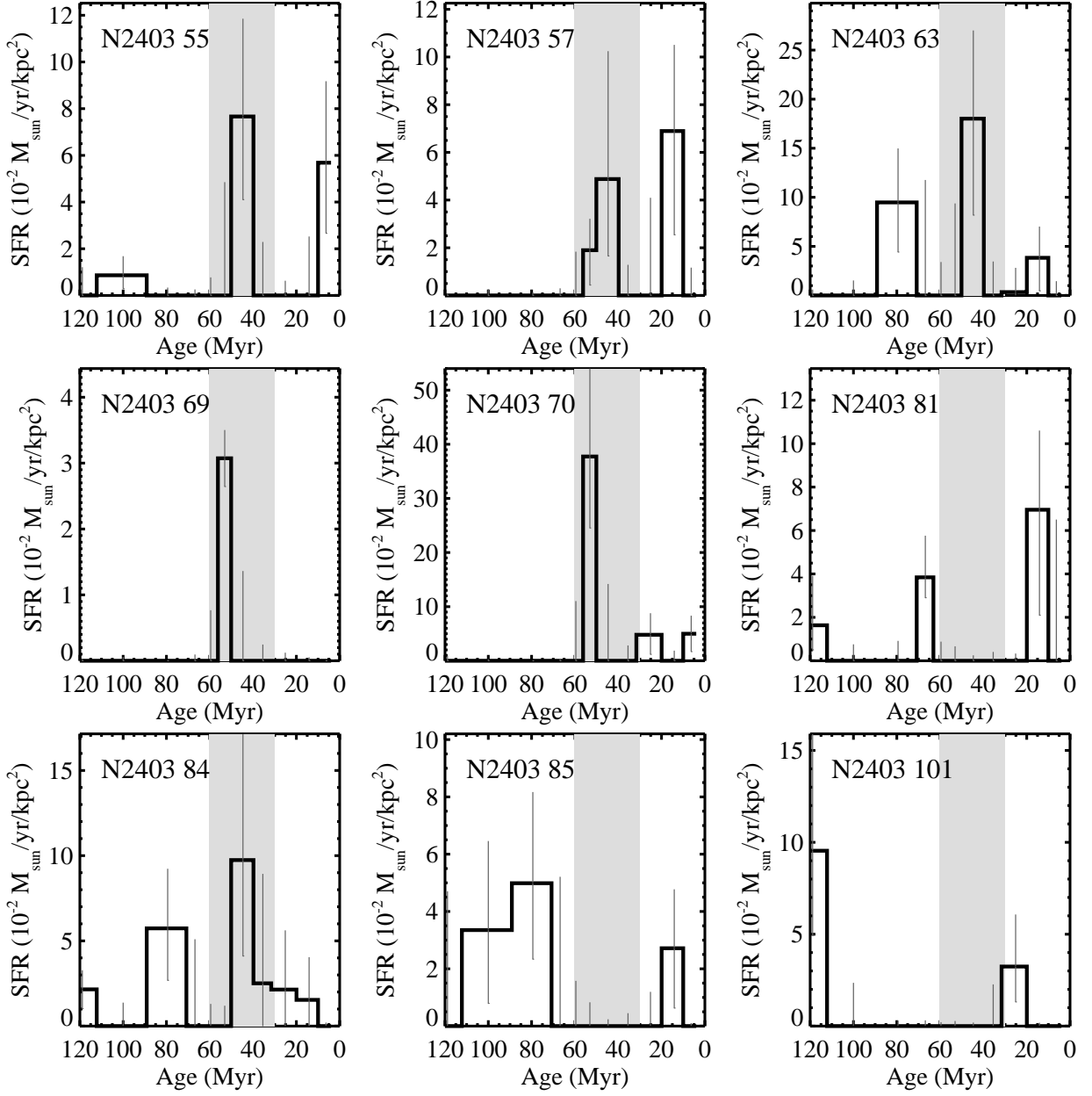


FIG. 5.— Same as Figure 4, but for the remaining 9 HMXB candidates shown in Figure 3.

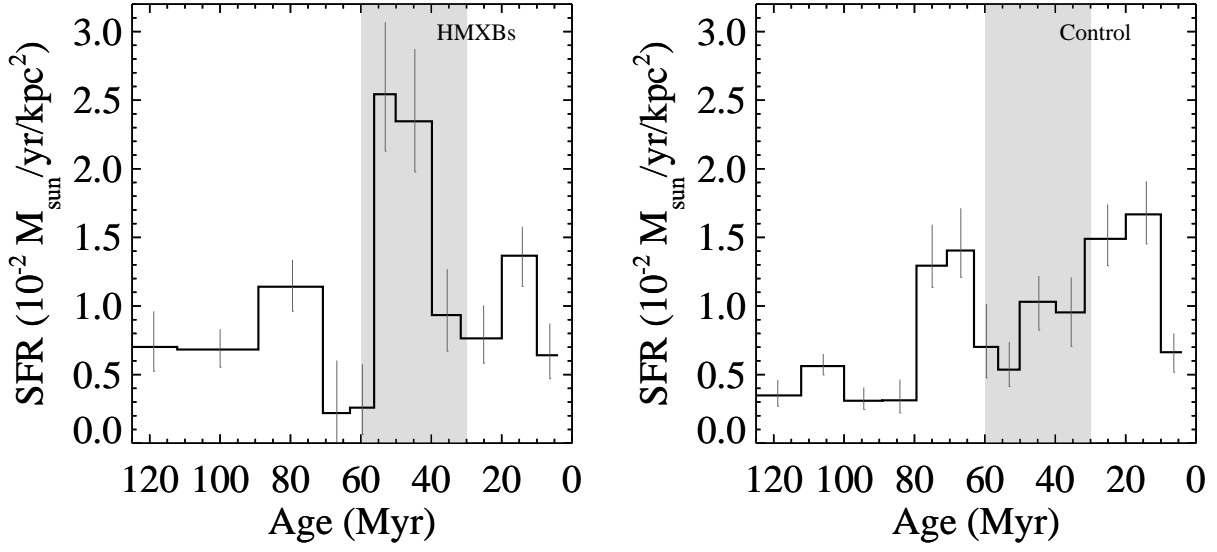


FIG. 6.— *Left*: Mean of all SFHs shown in Figure 4 and 5. *Right*: Mean of SFHs from 30 random locations in the *HST* fields used for the study.